

# RSC Advances



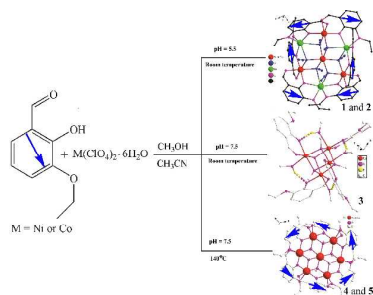
This is an *Accepted Manuscript*, which has been through the Royal Society of Chemistry peer review process and has been accepted for publication.

*Accepted Manuscripts* are published online shortly after acceptance, before technical editing, formatting and proof reading. Using this free service, authors can make their results available to the community, in citable form, before we publish the edited article. This *Accepted Manuscript* will be replaced by the edited, formatted and paginated article as soon as this is available.

You can find more information about *Accepted Manuscripts* in the [Information for Authors](#).

Please note that technical editing may introduce minor changes to the text and/or graphics, which may alter content. The journal's standard [Terms & Conditions](#) and the [Ethical guidelines](#) still apply. In no event shall the Royal Society of Chemistry be held responsible for any errors or omissions in this *Accepted Manuscript* or any consequences arising from the use of any information it contains.

Reported five novel clusters, the results show the pH and reaction temperatures play a key role in the self-assembly process.



# Structural Variation from Heterometallic Heptanuclear, Heptanuclear to Cubane Clusters Based on 2-hydroxy-3-ethoxy-benzaldehyde: Effects of pH and Temperature

Shu-Hua Zhang,<sup>a,\*</sup> Ru-Xia Zhao,<sup>a</sup> Gui Li,<sup>a</sup> Hai-Yang Zhang,<sup>a</sup> Chun-Lian Zhang,<sup>a</sup> Gilles Muller<sup>b,\*</sup>

<sup>a</sup>College of Chemistry and Bioengineering (Guangxi Key Laboratory of Environmental Friendly Electromagnetic Chemistry Function Materials), Guilin University of Technology, Guilin, People's Republic of China. 541004, email: zsh720108@163.com Telephone: +86 773 589 6839, Fax: +86 773 589 6839 (S. H. Zhang)

<sup>b</sup>Department of Chemistry, San José State University, One Washington Square, San José, CA 95192-0101, USA. email: gilles.muller@sjsu.edu, Telephone: 408 924 5000, Fax: 408 924 4945 (G. Muller).

**Abstract:** Five new Hheb complexes,  $\text{HN}(\text{C}_2\text{H}_5)_3 \cdot [\text{M}_4\text{Na}_3(\text{heb})_6(\mu_3\text{-N}_3)_6]$ , ( $\text{M} = \text{Ni}$  (**1**), and  $\text{Co}$  (**2**),  $[\text{Co}_4(\text{heb})_4(\mu_3\text{-OCH}_3)_4(\mu_1\text{-HOCH}_3)_4] \cdot (\text{H}_2\text{O})_2$  (**3**),  $[\text{M}_7(\text{heb})_6(\mu_3\text{-OCH}_3)_6] \cdot (\text{ClO}_4)_2$  ( $\text{M} = \text{Ni}$  (**4**), and  $\text{Co}$  (**5**), Hheb = 2-hydroxy-3-ethoxy-benzaldehyde), have been synthesized through reaction of hexahydrate perchlorate salt, Hheb, and  $\text{NaN}_3$  under different temperature and pH conditions. A careful investigation of the effect of the reaction temperature and pH resulted in a series of compounds with different compositions and nuclearities. The diverse compounds obtained illustrate the marked sensitivity of the structural chemistry of Co- or Ni-Hheb ligand-like systems to synthesis conditions. Complexes **1** and **2**, which are heterometallic heptanuclear anion  $[\text{M}_4\text{Na}_3(\text{heb})_6(\text{N}_3)_6]^-$  clusters, are formed at a pH of 5.5 and at room temperature. At a pH of 7.5 and at room temperature, a neutral molecular cubane cluster, namely **3**, is formed with a lower nuclearity. Further increase of the reaction temperature to 140°C at the same pH resulted to the formation of two heptanuclear cation  $[\text{M}_7(\text{heb})_6(\mu_3\text{-OCH}_3)_6]^{2+}$  clusters, **4** and **5**. The results show that the pH and reaction temperatures play a key role in the structural control of the self-assembly process. Interestingly, heterometallic heptanuclear anion  $[\text{M}_4\text{Na}_3(\text{heb})_6(\text{N}_3)_6]^-$  clusters have never been reported for the family of  $\mu_3\text{-N}_3^-$  or  $\mu_3\text{-O}$ -bridged heptanuclear clusters. The magnetic properties of **1-5** have been investigated and discussed in details.

Keywords: heptanuclear cluster, cubane cluster, magnetic properties, pH effect, reaction temperature

## INTRODUCTION

The rational design and synthesis of polynuclear complexes have undergone tremendous development because they have fascinating structures and functional applications such as optical, electronic, catalytic, fluorescent, and magnetic materials.<sup>1-4</sup> Particular interest has focused on the development of single molecule magnets (SMM).<sup>5</sup> An effective and facile approach for the synthesis of such complexes is still dependent on the suitable choice of well-designed organic ligands as bridge or terminal groups with metal ions or metal clusters as nodes. While a systematic, accurate prediction and total design of a crystal structure are not yet possible, efforts have been made to understand and control certain reaction parameters such as the metal-to-ligand molar ratio, the ligand denticity, the type of metal ions, the organic guest molecules, the presence of solvent molecules, the pH of the solution, the counter-ions, and the reaction temperatures that play crucial roles in the structure formation processes.<sup>2e,2f,6,7</sup> For examples, Li et al. reported that the pH does play a crucial role in the structure formation of 3,5-pyrazoledicarboxylic acid systems.<sup>6c,d</sup> Jacobson et al. reported that the reaction temperature and pH influence the coordination modes of the 1,4-benzenedicarboxylate ligand.<sup>6e</sup> In addition, our investigation on systems involving 2-Hydroxy-benzaldehyde ramification (HL)

ligands or (1H-benzimidazol-2-yl)-methanol ramification ligands has illustrated that the steric hindrance of the ligands does play a crucial role in the structure formation.<sup>2f,3f</sup> As part of our ongoing interest in understanding the effect of temperature and pH on the assembly of clusters, we have recently succeeded in the selective synthesis of five clusters by controlling the reaction temperature and pH. The details of the synthesis and characterization of these complexes with the multidentate ligand 2-hydroxy-3-ethoxy-benzaldehyde (Hheb, Scheme 1) are described in this paper.

### (Insert Scheme 1)

This ligand possesses three oxygen atoms from the phenoxo, aldehyde and C<sub>2</sub>H<sub>5</sub>O<sup>-</sup> groups and might be utilized as a versatile linker for the construction of interesting coordination polymers with abundant hydrogen bonds.<sup>2f,5a,8</sup> It is worth noting that the ligand 2-hydroxy-3-methoxy-benzaldehyde has been reported to possess four potential coordination modes comprising of  $\mu_5:\eta^2:\eta^2:\eta^1$ ,<sup>9</sup>  $\mu_2:\eta^1:\eta^1$ ,<sup>5a,10</sup>  $\mu_4:\eta^1:\eta^2:\eta^1$ ,<sup>2f,11</sup> and  $\mu_6:\eta^3:\eta^2:\eta^1$ ,<sup>12</sup> whereas its analogue, 2-hydroxy-3-ethoxy-benzaldehyde (Hheb), has just been reported to only show three coordination modes,  $\mu_2:\eta^1:\eta^1$ ,<sup>13</sup>  $\mu_4:\eta^1:\eta^2:\eta^1$ ,<sup>1e</sup> and  $\mu_5:\eta^2:\eta^2:\eta^1$ .<sup>14</sup> As a result, it was decided to investigate the coordination mode of the multidentate Hheb ligand with the objective to construct new clusters by controlling the temperature and pH during the preparation of these compounds.

## 2. Experimental

### 2.1. Materials and instrumentation

All chemicals were commercially available and used as received without further purification. Elemental analyses (CHN) were performed using an Elemental Vario-EL CHN elemental analyzer. FT-IR spectra were recorded from KBr pellets in the range of 4000–400 cm<sup>-1</sup> on a Bio-Rad FTS-7 spectrometer. The X-ray crystal structures were determined by single-crystal X-ray diffraction using the SHELXL crystallographic software for molecular structures. The PXRDs of **1-5** were determined by Rigaku D/max 2500v/pc. Magnetization measurements were carried out with a Quantum Design MPMS-XL7 SQUID to 50000 Oe for **1-5** ((HN(C<sub>2</sub>H<sub>5</sub>)<sub>3</sub>·[M<sub>4</sub>Na<sub>3</sub>(heb)<sub>6</sub>(μ<sub>3</sub>-N<sub>3</sub>)<sub>6</sub>] with M = Ni (**1**) and Co (**2**), [Co<sub>4</sub>(heb)<sub>4</sub>(μ<sub>3</sub>-OCH<sub>3</sub>)<sub>4</sub>(μ<sub>1</sub>-HOCH<sub>3</sub>)<sub>4</sub>]·(H<sub>2</sub>O)<sub>2</sub> (**3**), [M<sub>7</sub>(heb)<sub>6</sub>(μ<sub>3</sub>-OCH<sub>3</sub>)<sub>6</sub>]·(ClO<sub>4</sub>)<sub>2</sub> with M = Ni (**4**) and Co (**5**)). It must be mentioned that the  $\chi_M T$  vs  $T$  curves for all complexes of interest (except **3**) cannot be fitted by the Magpack method.

### 2.2. Syntheses

#### HN(C<sub>2</sub>H<sub>5</sub>)<sub>3</sub>·[Ni<sub>4</sub>Na<sub>3</sub>(heb)<sub>6</sub>(N<sub>3</sub>)<sub>6</sub>] (**1**)

A mixture of Ni(ClO<sub>4</sub>)<sub>2</sub>·6H<sub>2</sub>O (0.36 g, 1 mmol), NaN<sub>3</sub> (0.065, 1 mmol), Hheb (0.166 g, 1 mmol), acetonitrile (4 mL), and methanol (4 mL) with a pH adjusted to 5.5 by addition of triethylamine was stirred for 30 mins at room temperature. The resulting solution was left at room temperature and green crystals of **1** were obtained after 30 mins. The green crystals of **1** were collected by filtration, washed with methanol and dried in air. Phase pure crystals of **1** were obtained by manual separation (yield: 145 mg, *ca.* 52.72 % based on Hheb ligand). *Anal. Calc.* for **1**: C<sub>60</sub>H<sub>70</sub>N<sub>19</sub>Na<sub>3</sub>Ni<sub>4</sub>O<sub>18</sub> ( $M_r = 1649.08$ ), *calc.*: C, 43.69; H, 4.28; N, 16.13 %; Found: C, 43.57; H, 4.38; N, 16.19 %.. IR data for **1** (KBr, cm<sup>-1</sup>, Figure S1): 3439 w, 2978 w, 2087 s, 1618 s, 1550 m, 1442 s, 1346 m, 1216 s, 1102 m, 1006 w, 897 m, 747 m, 659 w, 577 w.

#### HN(C<sub>2</sub>H<sub>5</sub>)<sub>3</sub>·[Co<sub>4</sub>Na<sub>3</sub>(heb)<sub>6</sub>(N<sub>3</sub>)<sub>6</sub>] (**2**)

Complex **2** can be prepared in a similar way to **1**, except that Ni(ClO<sub>4</sub>)<sub>2</sub>·6H<sub>2</sub>O was replaced by Co(ClO<sub>4</sub>)<sub>2</sub>·6H<sub>2</sub>O. Red crystals of **2** were collected by filtration, washed with methanol and dried in air. Phase pure crystals of **2** were obtained by manual separation (yield: 142 mg, *ca.* 51.60 % based on Hheb ligand). *Anal. Calc.* For **2**: C<sub>60</sub>H<sub>70</sub>N<sub>19</sub>Na<sub>3</sub>Co<sub>4</sub>O<sub>18</sub> ( $M_r =$

1650.04), *calc*: C, 43.67; H, 4.28; N, 16.12 %; Found: C, 43.56; H, 4.41; N, 16.20 %. IR data for **2** (KBr,  $\text{cm}^{-1}$ , Figure S1): 3432 w, 2930 w, 2093 s, 1624 s, 1542 m, 1462 m, 1340 m, 1210 s, 1094 m, 1006 w, 904 m, 747 m, 645 w, 557w.

**[Co<sub>4</sub>(heb)<sub>4</sub>( $\mu_3$ -OCH<sub>3</sub>)<sub>4</sub>( $\mu_1$ -HOCH<sub>3</sub>)<sub>4</sub>](H<sub>2</sub>O)<sub>2</sub> (**3**)**

Complex **3** was prepared in a similar way to **2**, except that a pH of 7.5 was used instead of 5.5. Red crystals of **3**, which were obtained after 3 days, were collected by filtration, washed with methanol and dried in air. Phase pure crystals of **3** were obtained by manual separation (yield: 136 mg, *ca.* 45.92 % based on Hheb ligand). *Anal. Calcd.* For **3**: C<sub>44</sub>H<sub>68</sub>Co<sub>4</sub>O<sub>22</sub> (*M<sub>r</sub>* = 1184.70), *calc*: C, 44.61; H, 5.70 %; Found: C, 44.53; H, 5.79 %. IR data for **3** (KBr,  $\text{cm}^{-1}$ , Figure S1): 3433 m, 2814 w, 1632 s, 1536 m, 1428 m, 1332 w, 1238 m, 1204 s, 1053 m, 891 w, 741 m, 645 w, 565 w, 455m.

**[Ni<sub>7</sub>(heb)<sub>6</sub>( $\mu_3$ -OCH<sub>3</sub>)<sub>6</sub>](ClO<sub>4</sub>)<sub>2</sub> (**4**)**

Complex **4** was prepared in a similar way to **1**, except that the mixture was poured into a Teflon-lined autoclave (15 mL) and then heated at 140 °C for 5 days. Green crystals of **4** were collected by filtration, washed with methanol and dried in air. Phase pure crystals of **4** were obtained by manual separation (yield: 178 mg, *ca.* 69.72 % based on Ni ions). *Anal. Calcd.* For **4**: C<sub>60</sub>H<sub>72</sub>Cl<sub>2</sub>Ni<sub>7</sub>O<sub>32</sub> (*M<sub>r</sub>* = 1786.91), *calc*: C, 40.33; H, 4.06 %; Found: C, 40.23; H, 4.14 %. IR data for **1** (KBr,  $\text{cm}^{-1}$ , Figure S1): 3439 w, 3304 m, 2930 m, 1618 s, 1550 w, 1468 s, 1326 m, 1210 s, 1088 s, 891 w, 836 w, 741 m, 605 m.

**[Co<sub>7</sub>(heb)<sub>6</sub>( $\mu_3$ -OCH<sub>3</sub>)<sub>6</sub>](ClO<sub>4</sub>)<sub>2</sub> (**5**)**

Complex **5** can be prepared in a similar way to **4**, except that Ni(ClO<sub>4</sub>)<sub>2</sub>·6H<sub>2</sub>O was replaced by Co(ClO<sub>4</sub>)<sub>2</sub>·6H<sub>2</sub>O. Red crystals of **5** were collected by filtration, washed with methanol and dried in air. Phase pure crystals of **5** were obtained by manual separation (yield: 162 mg, *ca.* 63.40 % based on Co ions). *Anal. Calcd.* For **5**: C<sub>60</sub>H<sub>72</sub>Cl<sub>2</sub>Co<sub>7</sub>O<sub>32</sub> (*M<sub>r</sub>* = 1788.59), *calc*: C, 40.29; H, 4.06 %; Found: C, 40.21; H, 4.15 %. IR data for **5** (KBr,  $\text{cm}^{-1}$ , Figure S1): 3432 w, 3290 m, 2930 m, 2814 w, 1624 s, 1542 w, 1462 s, 1326 m, 1210 s, 1088 s, 884 m, 823 m, 735 m, 625 w, 577 m.

**Caution:** Perchlorate salts and azide of metal complexes with organic ligands are potentially explosive.

### 2.3. Crystal structure determination

The diffraction data were collected on an Agilent G8910A CCD diffractometer with graphite monochromated Mo-K $\alpha$  radiation ( $\lambda = 0.71073 \text{ \AA}$ ) and using the  $\omega$ - $\theta$  scan mode in the ranges  $2.97^\circ \leq \theta \leq 25.10^\circ$  (**1**),  $2.88^\circ \leq \theta \leq 25.01^\circ$  (**2**),  $2.89^\circ \leq \theta \leq 25.10^\circ$  (**3**),  $3.49^\circ \leq \theta \leq 25.08^\circ$  (**4**), and  $3.17^\circ \leq \theta \leq 25.05^\circ$  (**5**). Raw frame data were integrated with the SAINT program. The structures were solved by direct methods using SHELXS-97 and refined by full-matrix least-squares on  $F^2$  using SHELXS-97.<sup>15</sup> An empirical absorption correction was applied with the program SADABS.<sup>15</sup> All non-hydrogen atoms were refined anisotropically. All hydrogen atoms were positioned geometrically and refined as riding. Calculations and graphics were performed with SHELXTL.<sup>15</sup> The anisotropic displacement parameters of atoms C55-C60 in **1** and **2** were restrained to be identical with a standard uncertainty of  $0.01 \text{ \AA}^2$ . The structures contain solvent accessible voids of 250 and  $235 \text{ \AA}^3$  for **1** and **2**, respectively. The highest peak with  $1.340 \text{ e \AA}^{-3}$  of **3** and  $1.187 \text{ e \AA}^{-3}$  of **5** in the residual electron density are located  $0.09 \text{ \AA}$  from atom H6A and  $0.75 \text{ \AA}$  from atom H8B, respectively. The crystallographic details are provided in Table 1. Selected bond distances and angles for **1-5** are listed in Tables S1-S4 and Hydrogen Bond Lengths ( $\text{\AA}$ ) and Angles ( $^\circ$ ) in Complexes **1-3** are listed in Tables S5-S7. Crystallographic data for the structural analysis have been deposited with the Cambridge Crystallographic Data Center (CCDC reference numbers: 982504, 982505, 982508 – 982510).

Table 1. Crystallographic Data for Complexes 1-5.

Complexes	1	2	3	4	5
Formula	C <sub>60</sub> H <sub>70</sub> N <sub>19</sub> Na <sub>3</sub> Ni <sub>4</sub> O <sub>18</sub>	C <sub>60</sub> H <sub>70</sub> N <sub>19</sub> Na <sub>3</sub> Co <sub>4</sub> O <sub>18</sub>	C <sub>44</sub> H <sub>68</sub> Co <sub>4</sub> O <sub>22</sub>	C <sub>60</sub> H <sub>72</sub> Cl <sub>2</sub> Ni <sub>7</sub> O <sub>32</sub>	C <sub>60</sub> H <sub>72</sub> Cl <sub>2</sub> Co <sub>7</sub> O <sub>32</sub>
M <sub>r</sub>	1649.08	1650.04	1184.70	1786.95	1788.59
Crystal size (mm)	0.25×0.10×0.06	0.22×0.19×0.16	0.12×0.10×0.08	0.18×0.16×0.15	0.16×0.14×0.12
Crystal system	Monoclinic	Monoclinic	Tetragonal	Hexagonal	Hexagonal
Space group	<i>P</i> 2 <sub>1</sub> / <i>n</i>	<i>P</i> 2 <sub>1</sub> / <i>n</i>	<i>P</i> 4/ <i>ncc</i>	<i>P</i> $\bar{3}$	<i>P</i> $\bar{3}$
<i>a</i> (Å)	13.200 (1)	13.245 (1)	17.0166 (4)	14.649 (1)	14.818 (1)
<i>b</i> (Å)	26.664(1)	26.530 (1)	17.0166 (4)	14.649 (1)	14.818(1)
<i>c</i> (Å)	22.120 (1)	22.159 (1)	18.7995 (8)	9.663 (1)	9.391 (1)
$\alpha$ (°)	90	90	90	90	90
$\beta$ (°)	96.526 (3)	96.648 (3)	90	90	90
$\gamma$ (°)	90	90	90	120	120
<i>V</i> (Å <sup>3</sup> )	7735.1 (5)	7734.0(4)	5443.7 (3)	1795.7 (2)	1785.8 (3)
<i>F</i> (000)	3412	3396	2464	918	911
<i>Z</i>	4	4	4	1	1
<i>D</i> <sub>c</sub> (g cm <sup>-3</sup> )	1.417	1.418	1.446	1.652	1.663
$\mu$ (mm <sup>-1</sup> )	1.051	0.935	1.271	1.956	1.747
$\theta$ range (°)	2.97-25.10	2.88-25.01	2.89-25.10	3.49-25.08	3.17-25.05
Ref.meas./indep.	34163, 13773	58550, 13561	12303, 2432	3860, 2128	3653, 2111
Obs.ref. [ <i>I</i> >2 $\sigma$ ( <i>I</i> )]	8437	9059	1872	1602	1602
<i>R</i> <sub>int</sub>	0.0400	0.0565	0.0296	0.0210	0.0296
<i>R</i> <sub>1</sub> [ <i>I</i> ≥ 2 $\sigma$ ( <i>I</i> )] <sup>a</sup>	0.0549	0.0716	0.0543	0.0547	0.0566
$\omega R_2$ (all data) <sup>b</sup>	0.1797	0.2229	0.2013	0.1865	0.1657
Goof	1.002	1.070	1.009	1.008	1.008
$\Delta\rho$ (max,min)(eÅ <sup>-3</sup> )	0.707, -0.459	0.807, -0.605	1.340, -0.601,	0.830, -0.577	1.187, -0.677

<sup>a</sup>  $R_1 = \sum ||F_o| - |F_c|| / \sum |F_o|$ . <sup>b</sup>  $wR_2 = [\sum w(|F_o|^2 - |F_c|^2)|^2 / \sum w(|F_o|^2)]^{1/2}$

### 3. Results and discussion

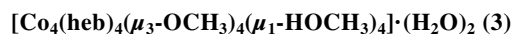
#### Description of the Crystal Structures

#### HN(C<sub>2</sub>H<sub>5</sub>)<sub>3</sub>·[M<sub>4</sub>Na<sub>3</sub>(heb)<sub>6</sub>(N<sub>3</sub>)<sub>6</sub>] (1 and 2)

The single-crystal X-ray diffraction analysis reveals that **1** and **2** are homeomorphism complexes and contain a heterometallic heptanuclear anion-type cluster,  $[M_4Na_3(heb)_6(\mu_3-N_3)_6]^-$ . Additionally, they represent the first  $\{M_4Na_3\}$  complexes to possess planar hexagonal disc-like structures. As illustrated in Figure 1, **1** consists of one wheel-like anion heterometallic heptanuclear cluster,  $[Ni_4Na_3(heb)_6(N_3)_6]^-$ , and one counter cation,  $HN(C_2H_5)_3^+$ . It can also be seen that the Ni1 atom located in the center of the structure is bridged by six  $\mu_3-N_3^-$  groups, which further are linked by three Ni atoms and three Na atoms on the rim that represents the bottom segment of the formed disc-like structure. The coordination geometry of the central Ni1 ion can be described as a slightly distorted octahedron with bond lengths of 2.107-2.138 Å and bond angles in the range of 79.3(2)-95.3(1)° (*cis*-angles) and 170.9(1)-171.9(2)° (*trans*-angles). On the rim, each Ni atom adopts a  $NiN_2O_4$  coordination configuration resulting from the coordination of two heb ligands and two  $\mu_3-N_3^-$  groups. The Ni atoms on the rim also formed distorted octahedral geometries as evidenced by the *cis*- and *trans*-angle values ranging between 79.9(1)-95.4(1)° and 170.7(14)-179.2(1)°, respectively. Coordinated bond lengths around the rim Ni atoms are in the range of 1.992(3)-2.134(4) Å. All Na atoms formed distorted trigonal bipyramid geometries with bond lengths of 2.232(4)-2.469(4) Å, which fall well within the range of Na-O distances of sodium complexes (Na-O distances are typically in the range of 2.234-2.609 Å).<sup>2a,16</sup> Therefore, heb, a hetero-multinucleating ligand, can coordinate to either a “soft” metal center ( $Ni^{2+}$ ) or a “hard” one ( $Na^+$ ). As such, the heb ligand, which displays a  $\mu_2:\eta^1:\eta^2:\eta^1$  coordination mode, is linked to one nickel and one sodium in the compound of interest (Scheme 1a). Although many heptanuclear clusters have been reported, e.g.,  $\{Ni_7\}$  clusters,<sup>17</sup>  $\{Mn_7\}$  cluster,<sup>18</sup>  $\{Zn_7\}$  clusters,<sup>17a,18e,19</sup>  $\{Fe_7\}$  clusters,<sup>18g,20</sup>  $\{Co_7\}$  clusters,<sup>2a,2e,21</sup> and  $\{M^II_6M^III\}$  ( $M = Co, Ni, Fe$ ),<sup>2f,20a,21e</sup> **1** and **2** represent the first high nuclear heterometallic heptanuclear anion clusters to the best of our knowledge (only a very limited number of anion-like clusters were reported in the literature).<sup>22</sup> It is interesting to mention that the counter ion  $HN(C_2H_5)_3^+$  is connected to the heterometallic heptanuclear anion cluster  $[M_4Na_3(heb)_6(\mu_3-N_3)_6]^-$  through N-H...N hydrogen bonds (N19-H19E...N6<sup>i</sup>, 2.938(9) Å, symmetry code: (i)  $x - 1, y, z$ , Table S5). All azide ligands in **1** and **2** are linear, herein, the N–N–N bond angles range from 176.3(6) to 179.1(8)°. The N–N bond lengths of the *azide* ligands are distinguishable from those of Ni(II) complexes containing end-on doubly bridging azides.<sup>23</sup> It can also be seen that the heb ligand-based clusters **1** and **2** show that the expansion direction of the heb ligands is different than the one observed in other heptanuclear clusters constructed by 2-hydroxy-benzaldehyde ramifications.<sup>2a,2f,17c</sup> This is most likely due to the fact that each pair of heb ligands faces each other instead of being directed in the same direction as typically found for the 2-hydroxybenzaldehyde-type heptanuclear clusters. This difference may be attributed to the type of rings that can be formed in these clusters. It is well known that in compounds with 2-hydroxy-benzaldehyde ramifications, the phenoxo and aldehyde groups form a six-member ring with the metal ion, whereas phenoxo and RO- groups lead to a more open five-member ring. As a result, a more open five-member ring would facilitate the incorporation and coordination of the Na ion than in a system comprising a six-member ring. Thus, this finding may open new perspectives in a better design of cluster-type systems.

(Insert Scheme 2)

(Insert Figure 1)



The single-crystal X-ray crystallographic analysis reveals that **3** contains a methoxy anion bridged discrete cubane-based cluster of formula  $[Co_4(heb)_4(\mu_3-OCH_3)_4(\mu_1-HOCH_3)_4] \cdot (H_2O)_2$  (Figure 2). There is one independent Co(II) ion, assuming a distorted octahedral geometry with *cis*-angles O–Co–O in the range of 80.5–99.0° and Co–O bonds of 2.034(3)–2.156(4) Å from three  $\mu_3$ -OMe, a chelating heb, and one MeOH. The adjacent Co...Co distances and the Co–O–Co angles are in the range of

3.093–3.193 Å and 94.7–99.5°, respectively. It is worthwhile noting that heb exists as a mono-anion and bonds *via* a  $\mu_1:\eta^1:\eta^1$  coordination mode (Scheme 1b). Additionally, intramolecular hydrogen bonds exist between adjacent phenolato oxygen atoms and the proton from the MeOH molecule with distances of 2.764 Å across four of the six faces of the cubane (Table S3). As a result, these four faces exhibit shorter Co...Co distances (3.090 Å) and smaller magnetic exchange Co–O–Co angles (94.7, 95.5°). Thus, **3** displays an approximate  $S_4$  site symmetry, while the exact crystallographic point symmetry is  $C_1$ .

(Insert Figure 2)

As shown in Figure S2, the different cubes present in the cluster are well separated from each other by the heb ligands and methoxy groups resulting in cent-cent distances of adjacent cubanes of 9.40 Å in the *c* direction and 12.03 Å in the *ab* plan of intramolecular hydrogen bonds. Moreover, the nearest intercluster Co...Co distances are 9.464 Å in the *ab* plan and 7.41 Å in the *c* direction.

#### **[M<sub>7</sub>(heb)<sub>6</sub>( $\mu_3$ -OCH<sub>3</sub>)<sub>6</sub>](ClO<sub>4</sub>)<sub>2</sub> (**4,5**)**

Since the single-crystal X-ray diffraction analysis also confirms that **4** and **5** are homeomorphism complexes and contain a heterometallic heptanuclear cation-type cluster,  $[M_7(\text{heb})_6(\mu_3\text{-OCH}_3)_6]^{2+}$ , only **4**, which belongs to the trigonal space group *P*-3, will be discussed in details. Its unit cell contains one disc-like heptanuclear nickel cluster  $[\text{Ni}_7(\text{heb})_6(\mu_3\text{-OCH}_3)_6]^{2+}$  and two counter anions  $\text{ClO}_4^-$ , which lie on a site with a threefold symmetry (Figure 3). In addition, six  $\mu_2$ -phenoxo groups bridge the six nickel ions on the rim, which are linked to the central nickel ion through six  $\mu_3$ -OCH<sub>3</sub> bridging groups. It must be noted that these latter act as the ‘bottom’ segment in the formed disc-like structure. The coordination geometry of the central nickel ion (Ni2) can be described as a slightly distorted octahedron with bond lengths of 2.077(3) Å (Ni2-O4) and O-Ni2-O angles in the range of 82.2(2)–97.8(2)° (*cis*-angles), whereas all of the *trans*-angles have a value of 180.0°. Each nickel ion on the rim (Ni1) adopts a NiO<sub>6</sub> configuration since Ni1 is coordinated by four O atoms from two different heb ligands and two O(O4, O4b) atoms from two methoxy groups resulting in the formation of a slightly distorted octahedral geometry (Ni1-O1, 1.990(4); Ni1-O1a, 1.997(4); Ni1-O2a, 2.029(5); Ni1-O4b, 2.045(4); Ni1-O4, 2.076(4) and Ni1-O3, 2.345(4) Å; symmetry code: (a) *x* - *y*, *x*, 2 - *z* and (b) *y* - *x*, - *x*, 2 + *z*). The O-Ni1-O angles lie in the range of 72.4(2)–104.7(2)° and 151.9(2)–172.8(1)° for the *cis*- and *trans*-angles, respectively. Additionally, the magnetic exchange angles of Ni-O-Ni are in the range of 96.8(2)–102.6(2)°. It must be pointed out that the assignment of the metal ions on the rim (Ni1) and at the center (Ni2) of the structure was based on the valence sum calculation. The heb anionic ligands, which bridge the peripheral Ni<sup>II</sup> centers, display a  $\mu_2:\eta^1:\eta^2:\eta^1$  coordination mode (Scheme 2c) and lie alternately above and below the {Ni<sup>II</sup>} plane. Moreover, the packing mode for **4** and **5** can be described as AAA along the *c* axis as shown for instance in the packing diagram of **4** (Fig. S3). The disc-like Ni<sub>7</sub> units are well separated from each other by heb ligands, methoxy groups and  $\text{ClO}_4^-$  ions, and thus resulting in center distances between adjacent clusters of 14.65 Å and 14.82 Å in the *ab* plane, and 9.66 and 9.39 Å in the *c* direction for **4** and **5**, respectively (Fig. S3). On the other hand, the core of the cluster can be described as an almost planar {Ni<sub>6</sub>} moiety (a ±0.1143 Å deviation from the average plane), which is composed by [Ni1] and its five centrosymmetric equivalent Ni atoms, and where the central nickel ion (Ni2) lies on a site with a threefold symmetry. Although the structural motif belongs to the increasing {M<sub>7</sub>} family,<sup>17-21</sup> it is worth mentioning that only a few heptanuclear clusters have been reported so far,<sup>17-21</sup> but more importantly **5** is the first example for 2-hydroxy-3-ethoxy-benzaldehyde cobalt cluster to the best of our knowledge.

(Insert Figure 3)

#### **Structural and Synthetic Aspects**

Our aim is to investigate the effects of the temperature and pH on the self-assembly of supramolecules and clusters. Co(II), Ni(II), and Hheb were selected as starting materials in our study. The synthetic strategy for the Hheb system is depicted in Scheme 2. Complexes **1-3** were obtained under similar conditions with the exception of the pH. At first, we carried out the complex synthesis at a pH of 5.5 and at room temperature, and compounds **1** and **2** with heterometallic heptanuclear anion  $[M_4Na_3(heb)_6(N_3)_6]^-$  clusters were obtained. When the pH of the reaction was raised to 7.5, complex **3** with a cubane cluster was obtained. It is interesting to note that the anionic group  $N_3^-$  is not present in **3** unlike it was seen for **1** and **2**. On the basis of the synthetic conditions used to prepare **1-3**, it can be concluded that the pH conditions are most likely responsible for the structural differences observed between **1**, **2**, and **3**. In addition to affect the deprotonation of the organic ligands used in the formation of the three complexes, an increase in the pH conditions also results in the presence of solvent anionic species such as  $CH_3O^-$  at higher pH (7.5). As a result, the methanol molecules exist under the form of  $CH_3O^-$  anionic species which can be coordinated as  $\mu_3-OCH_3$  in **3** when a pH of 7.5 is used. On the other hand, the methanol molecules only function as solvent species in the formation of **1** and **2** when the pH is maintained at 5.5. It must be mentioned that a different single crystal growth time was used for the formation of the three complexes, which would also affect the type of systems obtained. The single crystal growth time was about 30 minutes for **1** and **2**, whereas a much longer time was required for **3** (three days).

In addition to the pH effect, the temperature has also an influence on the type of the compounds obtained. Increasing the temperature from room temperature to 140 °C resulted in the formation of the two heptanuclear cationic  $[M_7(heb)_6(\mu_3-OCH_3)_6]^{2+}$  clusters **4** and **5** when the pH was adjusted with triethylamine to 7.5. In comparison with **3**, which was synthesized at room temperature, the findings regarding **4** and **5** show that the solvothermal temperature also plays an important role in the formation of different clusters (e.g., **1-5**). According to the above discussion and considering the comparison of **1** and **2** with **3**, we can conclude that a lower pH (5.5) is necessary for the coordination of azide ions while a higher pH (7.5) is needed for the presence of  $CH_3O^-$  anions in the solution, which can then coordinate as  $\mu_3-OCH_3$  species in **3**. At the same time, comparing **3** and **4** with **5**, we can conclude that lower temperatures (room temperature) and higher temperatures (140 °C) may result in the formation of lower and higher nuclear complexes, respectively. This can be explained most likely by the increase of the degree of condensation of metal polyhedra and the ligand coordination ability when the reaction temperature is increased.<sup>6e,7f,24</sup>

Furthermore, it was decided to investigate the influence of the bulky ethyl group on the formation of such self-assembly systems. As such, 2-hydroxy-3-methoxy-benzaldehyde (Hhmb) was used instead of 2-hydroxy-3-ethoxy-benzaldehyde under the same experimental conditions as **1** and **2**. It is worth noting that the two obtained compounds that result in the formation of two heterometallic  $[M_2Na_2(\mu_{1,1,1}-N_3)_2(hmb)_4(CH_3CN)_2] \cdot (CH_3CN)_2$  ( $M = Ni$  (**a**)<sup>25</sup>,  $M = Co$  (**b**)<sup>26</sup>, Figure S4) clusters with two face-sharing cubes (each with one vertex missing) were different than the ones expected,  $(HN(C_2H_5)_3) \cdot [M_4Na_3(hmb)_6(N_3)_6]$ . It is most likely due to the fact that Hhmb and Hheb present different coordination abilities resulting presumably from the steric hindrance of the RO groups, even if the phenolic hydroxyl, aldehyde, and RO- groups comprised in the coordination sites of Hhmb and Hheb are very similar.

### **Magnetic properties**

The magnetic susceptibilities of **1-5** were measured from crushed single crystalline samples (the phase purity of **1-5** have been checked by PXRD patterns, see Figure S5), and variable-temperature direct-current (dc) magnetic susceptibility data were collected for **1-5** in the temperature range of 2-300 K under an applied field of 1000 Oe.

### **Magnetic properties of 1 and 4**

For complexes **1** and **4**, spin-orbital coupling of Ni(II) ions gives rise to a value of the  $\chi_m T$  product of 5.84  $cm^3 K mol^{-1}$  (**1**) and 9.13  $cm^3 K mol^{-1}$  (**4**) at room temperature (Figure 4). This behavior suggests an orbital contribution of the distorted octahedral

Ni(II) ions. For **1**, this value is higher than the calculated spin-only value of  $4.4 \text{ cm}^3\text{Kmol}^{-1}$  from four non-interaction high-spin Ni(II) ions assuming  $g = 2.2$ . It must be noted that the observed value of **1** is also slightly higher than what was obtained for  $[\text{Ni}_4(\text{ROH})_4\text{L}_4]$  ( $\text{H}_2\text{L} = \text{salicylidene-2-ethanolamine}$ ;  $\text{R} = \text{Me}$  or  $\text{Et}$ ) ( $\sim 5.1 \text{ cm}^3\text{Kmol}^{-1}$ )<sup>27</sup> and  $[\text{Ni}_4(\mu_3\text{-OMe})(\text{MeOH})_4\text{L}_4]$  ( $\text{H}_2\text{L}$  is 2-hydroxy-3-methoxybenzaldehyde) ( $\sim 5.45 \text{ cm}^3\text{Kmol}^{-1}$ ),<sup>5a</sup> but smaller than for  $[\text{HN}(\text{C}_2\text{H}_5)_3]_8 \cdot [\text{Ni}_4(\text{dchaa})_4(\text{N}_3)_4]_2$  ( $\text{dchaa}$  is the anion of 3,5-dichloro-2-hydroxy-benzylaminoacetic acid) ( $\sim 6.54 \text{ cm}^3\text{Kmol}^{-1}$ ).<sup>22b</sup> The  $\chi_{\text{m}}T$  value of **1** at room temperature lies in the range of other tetranuclear nickel clusters, which have  $\chi_{\text{m}}T$  values between  $5.1$  and  $6.61 \text{ cm}^3\text{Kmol}^{-1}$ .<sup>5a,22b,28,29</sup> Upon decreasing  $T$ , the  $\chi_{\text{m}}T$  products of **1** and **4** gradually increases to a maximum value of  $14.67$  and  $10.13 \text{ cm}^3\text{Kmol}^{-1}$  at  $35 \text{ K}$ , and then smoothly fall to  $5.7$  and  $7.47 \text{ cm}^3\text{Kmol}^{-1}$  at  $2 \text{ K}$ , respectively. It is noteworthy to mention that similar magnetic behaviors were observed for  $[\text{Ni}_4(\text{ROH})_4\text{L}_4]$ ,<sup>27</sup>  $[\text{Ni}_4(\mu_3\text{-OMe})(\text{MeOH})_4\text{L}_4]$ ,<sup>5a</sup>  $[\text{Ni}_4(\eta^1, \mu_3\text{-N}_3)_4(\text{dbm})_4(\text{EtOH})_4] \cdot 2\text{C}_7\text{H}_8$  ( $\text{Hdbm}$  is dibenzoylmethane),<sup>28</sup> and  $[\text{Ni}_7(\text{mmimp})_6(\text{CH}_3\text{O})_6] \cdot (\text{X})_2$ .<sup>17c</sup> The sudden decrease of  $\chi_{\text{m}}T$  is assigned to zero-field splitting in the ground state, Zeeman effects, or intercluster antiferromagnetic interactions at low temperatures.

#### (Insert Figure 4)

The temperature dependence of the reciprocal susceptibility  $\chi_{\text{M}}^{-1}$  above  $50 \text{ K}$  follows the Curie–Weiss law [ $\chi = C/(T - \theta)$ ] with Weiss and Curie constants of  $39.34(1) \text{ K}$  and  $5.18(1) \text{ cm}^3\text{Kmol}^{-1}$  for **1** and  $5.18(1) \text{ K}$  and  $9.01(1) \text{ cm}^3\text{Kmol}^{-1}$  for **4**, respectively (Figure S6a,d). The larger positive Weiss constants suggest an intramolecular ferromagnetic interaction between adjacent Ni(II) ions through the  $\mu_3\text{-N}_3$  and  $\mu_3\text{-O}$  bridges in **1** and **4**. For **1**, the observation of a maximum of  $\chi_{\text{M}}T$  at  $35 \text{ K}$  is indicative of an  $S = 4$  ground state (with  $g = 2.25$ ,  $\chi_{\text{M}}T = 0.125g^2S_{\text{T}}(S_{\text{T}} + 1) \approx 12.66 \text{ cm}^3\text{Kmol}^{-1}$ ). As such, this pattern is compatible with a moderate ferromagnetic coupling.<sup>29</sup> Further evidence of ferromagnetic coupling between Ni(II) ions was observed in the variable-field magnetization curves plotted in Figure S7a,d. At low fields from  $0$  to  $10000 \text{ Oe}$ , the magnetization of **1** and **4** sharply increases. For **1**, above  $10000 \text{ Oe}$ , the magnetization slowly increases and saturates at  $8.85 \text{ N}\mu\text{B}$  when a field of  $50000 \text{ Oe}$  is achieved, which is consistent with  $M = gS_{\text{T}} = 2.22 \times 4 = 8.88 \text{ N}\mu\text{B}$ . For **4**, above  $10000 \text{ Oe}$ , it slowly increases but does not saturate at  $50000 \text{ Oe}$ . Finally, AC susceptibility measurements were carried out in the  $2\text{--}10 \text{ K}$  range at frequencies of  $10 \text{ Hz}$ ,  $100 \text{ Hz}$ ,  $300 \text{ Hz}$ , and  $997 \text{ Hz}$  for **1** and  $100$ ,  $997 \text{ Hz}$  for **4** (Figure S8a,d). The result of these measurements confirmed that **1** and **4** do not behave as a SMM which is corroborated by the fact that no out-of-phase ac signals were observed above  $2 \text{ K}$ .

#### Magnetic properties of 2, 3, and 5

As seen for **1**, the complexes **2**, **3**, and **5** show that, at room temperature, the spin-orbital coupling of the Co(II) ions gives rise to a  $\chi_{\text{m}}T$  product of  $12.53$ ,  $9.15$ , and  $31.85 \text{ cm}^3\text{Kmol}^{-1}$  for **2**, **3**, and **5**, respectively (Figure 5). For **2** and **3**, the obtained values are much higher than the calculated spin-only value of  $7.5 \text{ cm}^3\text{Kmol}^{-1}$  from four non-interacting high-spin Co(II) ions, assuming  $g = 2.0$ .<sup>5a,30</sup> On the other hand, **5** shows that the  $\chi_{\text{m}}T$  value is much higher than the calculated spin-only value ( $13.1 \text{ cm}^3\text{Kmol}^{-1}$ ) of seven high-spin non-interacting Co(II) ions with the assumption that  $g$  is equal to  $2.0$ .<sup>21h</sup> These findings can be explained by the orbital contribution to the magnetic moment of Co(II). For **2**, with decreasing  $T$ ,  $\chi_{\text{m}}T$  gradually rises to a local maximum of  $20.08 \text{ cm}^3\text{Kmol}^{-1}$  at  $14 \text{ K}$  before falling to  $8.38 \text{ cm}^3\text{Kmol}^{-1}$  at  $2 \text{ K}$ . It must be pointed out that the characteristic pattern consisting in a significant decrease in the value of  $\chi_{\text{m}}T$  as the temperature is lowered is often observed for Co(II) complexes due to a strong orbital contribution, is in fact not seen for **2**.<sup>31</sup> This can be explained by the fact that (i) the orbital contribution is partially quenched due to the distortions from the typical octahedral symmetry at the Co(II) centers and (ii) the increase in  $\chi_{\text{m}}T$  below  $37 \text{ K}$  due to the ferromagnetic exchange interactions between the Co(II) centers. This is consistent with a similar magnetic behavior that was observed for a  $\text{Co}_{12}$  wheel.<sup>32</sup> For **3**, the  $\chi_{\text{M}}T$  value slowly falls off upon cooling to a value of  $8.5 \text{ cm}^3\text{Kmol}^{-1}$  at  $60 \text{ K}$ , after which it rapidly decreases to  $4.23 \text{ cm}^3\text{Kmol}^{-1}$  when a temperature of  $2 \text{ K}$  is achieved. This pattern most likely indicates the

occurrence of a relatively weak antiferromagnetic intra-cluster interaction between the four Co(II) ions. For **5**, the  $\chi_M T$  value decreases gradually and reaches a minimum of  $30.05 \text{ cm}^3\text{Kmol}^{-1}$  at 40 K (Figure 5). In the range of 300 to 40 K, the magnetic properties of **5** mainly exhibit single-ion behavior of the Co(II) ion. Below 40 K, it can be suggested that the pattern observed (a slight increase of the  $\chi_M T$  value up to a maximum of  $31.37 \text{ cm}^3\text{Kmol}^{-1}$  at 14 K, and then a sharp decrease to  $9.87 \text{ cm}^3\text{Kmol}^{-1}$  at 2 K) is the consequence of the fact that the ferromagnetic coupling between the Co(II) ions offsets the effect of the spin-orbital coupling, and thus compensates the decrease of the  $\chi_M T$  value. This is consistent with a similar magnetic behavior observed for  $[\text{Co}_7(\text{bzip})_6(\text{N}_3)_9(\text{CH}_3\text{O})_3](\text{ClO}_4)_2 \cdot 2\text{H}_2\text{O}$ ,<sup>33</sup>  $[\text{Co}^{\text{II}}_4\text{Co}^{\text{III}}_3(\text{HL})_6(\text{NO}_3)_3(\text{H}_2\text{O})_3]^{2+}$  ( $\text{H}_3\text{L} = \text{H}_2\text{NC}(\text{CH}_2\text{OH})_3$ ),<sup>21c</sup>  $\text{Co}_{12}$  wheel,<sup>32</sup> and  $[\text{Co}_7(\text{immp})_6(\text{CH}_3\text{O})_6](\text{ClO}_4)_2$  (immp is 2-iminomethyl-6-methoxy-phenolic anion).<sup>2a</sup>

The temperature dependence of the reciprocal susceptibility  $\chi_M^{-1}$  above 50 K follows the Curie–Weiss law [ $\chi = C/(T - \theta)$ ] with Weiss and Curie constants of 5.00(1) K and  $12.56(1) \text{ cm}^3\text{Kmol}^{-1}$ , -4.29 (1) K and  $9.33 (1) \text{ cm}^3\text{Kmol}^{-1}$ , and -1.98 K and  $32.39 \text{ cm}^3\text{Kmol}^{-1}$  for **2**, **3**, and **5**, respectively (Figure S6b,c,e). Compared to **3** and **5**, the larger positive Weiss constant observed for **2** also suggests an intramolecular ferromagnetic interaction between adjacent Co(II) ions through the  $\mu_3\text{-N}_3$  bridges, whereas the maximum of  $\chi_M T$  at 14 K is indicative of an  $S = 6$  ground state (with  $g = 2.00$ ,  $\chi_M T = 0.125g^2S_T(S_T + 1) \approx 21 \text{ cm}^3\text{Kmol}^{-1}$ ). Similarly, the larger negative Weiss constant observed for **3** compared to **1** and **5** suggests dominant intramolecular anti-ferromagnetic interactions between adjacent Co(II) ions through the  $\mu_3\text{-O}$  bridges. Finally, the contribution of a spin–orbital interaction discussed earlier has also an effect on the ferromagnetic exchange occurring in **5** (it is diminished). As a result, a smaller negative value of the Weiss constant was obtained. Further evidence of ferromagnetic coupling between Co(II) ions in **2**, **3**, and **5** was observed in the variable-field magnetization curves plotted in Figure S7b,c,e. At low fields from 0 to 10000 Oe, the magnetization sharply increases, whereas above 10000 Oe, the magnetization slowly increases but does not saturate at 50000 Oe for **2** and **3**. This is different from what was observed for **5** since above 10000 Oe the magnetization slowly increases and then saturates to  $23.40 N\mu\beta$  at 50000 Oe, which is consistent with  $M = gS_T = 2.22 \times 21/2 = 23.31 N\mu\beta$ . Furthermore, the AC susceptibility measurements that were carried out in the 2–10 K range at frequencies of 100 Hz and 997 Hz (for **2** and **5**), and 10, 100, 300, 600, 997 Hz for **3** (Figure S8b,c,e) suggested that **2**, **3**, and **5** do not behave as a SMM since no out-of-phase ac signals were detected above 2 K.

#### (Insert Figure 5)

According to the cubic structure of the cluster, the magnetic exchange between Co(II) ions in the core of  $\text{Co}_4\text{O}_4$  observed for **3** can be assessed by using the Van Vleck's equation (eqn.1). This is based on the Kambe's method which requires the use of the isotropic spin Hamiltonian  $\hat{H} = -2J_1 \sum_{i \neq j=1}^4 \hat{S}_i \hat{S}_j$  and where  $J_1$  is the coupling constant between the Co(II) ions.

$$\chi = \frac{2Ng^2\beta^2}{kT} \times \frac{e^{2J_1/kT} + 5e^{4J_1/kT} + e^{-4J_1/kT} + 14e^{6J_1/kT}}{3e^{2J_1/kT} + e^{-2J_1/kT} + 5e^{4J_1/kT} + 3e^{-4J_1/kT} + 7e^{6J_1/kT}} \quad (\text{eqn.1})$$

The best fitting in the temperature range of from 300 to 50 K gave  $g = 2.21$  and  $J_1 = -0.87(1) \text{ cm}^{-1}$  with  $R = 1.9 \times 10^{-4}$ . The negative coupling constant indicates a relatively weak anti-ferromagnetic intracube Co(II) interaction, which is different from those observed in several related octahedral Co(II) complexes with similar cuboidal cores.<sup>5a,34</sup>

#### Conclusions

Five new polynuclear clusters have been synthesized by modulating the pH and reaction temperature conditions. The results show that these two factors play a key role in the structural control of the self-assembly process. Additionally, the magnetic studies indicate that **1**, **2**, **4**, and **5** display dominant ferromagnetic intracube interactions whereas **3** displays an anti-

ferromagnetic interaction between Co(II) ions. Subsequent works will be focused on the construction of novel polymers using 2-hydroxy-3-ethoxy-benzaldehyde as a basic building unit.

### Acknowledgements

This work is financially supported by the National Nature Science Foundation of China (No. 21161006), Program for Excellent Talents in Guangxi Higher Education Institutions (Gui Jiao Ren [2012]41). G.M. thanks the Henry Dreyfus Teacher-Scholar Award for financial support.

### Notes and references

†CCDC 982504-982510 contain the supplementary crystallographic data for complexes **1–5** and **a, b**. These data can be obtained free of charge via <http://www.ccdc.cam.ac.uk/conts/retrieving.html>, or from the Cambridge Crystallographic Data Centre, 12 Union Road, Cambridge CB2 1EZ, UK; fax: (+44) 1223-336-033; or e-mail: [deposit@ccdc.cam.ac.uk](mailto:deposit@ccdc.cam.ac.uk). Electronic supplementary information (ESI) available: the IR of **1–5**. Packing drawing of **3–5**. The structures of **a** and **b**. The PXRDs of **1–5**. The plots of  $\chi_M^{-1}$  vs  $T$  of **1–5**. The plots of  $M-H$  of **1–5**. The plots of  $\chi''$  and  $\chi'$  vs  $T$  of **1–5**.

### References

- (a) C. S. Liu, X. S. Shi, J. R. Li, J. J. Wang, X. H. Bu, *Cryst. Growth Des.* 2006, **6**, 656–663. (b) B. Zhao, H. L. Gao, X. Y. Chen, P. Cheng, W. Shi, D. Z. Liao, S. P. Yan, Z. H. Jiang, *J. Eur. Chem.* 2006, **12**, 149–158. (c) S. Hu, F. Y. Yu, P. Zhang, D.R. Lin, *Dalton Trans.* 2013, 42, 7731–7740; (d) S. Hu, F. Y. Yu, P. Zhang, A. J. Zhou, *Eur. J. Inorg. Chem.*, 2012, 3669–3673. (e) S. H. Zhang, R. X. Zhao, H. P. Li, C. M. Ge, Q. P. Huang, H. H. Zou, *J. Solid State Chem.* 2014, **216**, 30–35.
- (a) S. H. Zhang, Y. Song, H. Liang, M. H. Zeng, *CrystEngComm* 2009, **11**, 865–872. (b) Y. Xiao, P. Huang, W. Wang, *J. Clust. Sci.*, 2014, doi:10.1007/s10876-014-0799-9. (c) B. Q. Ma, D. S. Zhang, S. Gao, T. Z. Jin, C. H. Yan, *Angew. Chem. Int. Ed.* 2000, **39**, 3644–3946; (d) L. F. Ma, L. Y. Wang, Y. Y. Wang, S. R. Batten, J. G. Wang, *Inorg. Chem.* 2009, **48**, 915–924. (e) S. H. Zhang, L. F. Ma, H. H. Zou, Y. G. Wang, H. Liang, M. H. Zeng, *Dalton Trans.* 2011, **40**, 11402–11409. (f) S. H. Zhang, N. Li, C. M. Ge, C. Feng, L. F. Ma, *Dalton Trans.* 2011, **40**, 3000–3007.
- (a) R. Q. Zou, H. Sakurai, Q. Xu, *Angew. Chem. Int. Ed.* 2006, **45**, 2542–2546. (b) P. Li, H. M. Liu, X. G. Lei, X. Y. Huang, D. H. Olson, N. J. Turro, J. Li, *Angew. Chem. Int. Ed.* 2003, **42**, 542–546. (c) J. S. Seo, D. Whang, H. Lee, S. I. Jun, J. Oh, Y. J. Jeon, K. Kim, *Nature* 2000, **404**, 982–986. (d) S. Hu, P. Zhang, F. Y. Yu, M. X. Chen, D. R. Lin, *Polyhedron* 2014, **67**, 388–395. (f) L. Yang, S.-H. Zhang, W. Wang, J.-J. Guo, Q. P. Huang, R.-X. Zhao, C.-L. Zhang and G. Muller, *Polyhedron*, 2014, **74**, 49–56.
- M. Fujita, A. Powell, C. Creutz, *From the molecular to the nanoscale: synthesis, structure, and properties*, Elsevier Ltd., Oxford, 2004, Vol. 7, 1–56.
- (a) S. H. Zhang, Y. D. Zhang, H. H. Zou, J. J. Guo, H. P. Li, Y. Song, H. Liang, *Inorg. Chim. Acta*, 2013, **396**, 119–125. (b) E. Tancini, M. Mannini, P. Sainctavit, E. Otero, R. Sessoli, A. Cornia, *Chem. Eur. J.* 2013, **19**, 16902–16905. (c) M. Dey, N. Gogoi, *Angew. Chem. Int. Ed.* 2013, **52**, 12780–12782. (d) D. Aravena, E. Ruiz, *Inorg. Chem.* 2013, **52**, 13770–13778. (e) F. Habib, G. Brunet, V. Vieru, I. Korobkov, L. F. Chibotaru, M. Murugesu, *J. Am. Chem. Soc.*, 2013, **135**, 13242–13245. (f) A. Deb, T. T. Boron, III, M. Itou, Y. Sakurai, T. Mallah, V. L. Pecoraro, J. E. Penner-Hahn, *J. Am. Chem. Soc.*, 2014, **136** (13), 4889–4892. (g) R. A. Layfield, *Organometallics*, 2014, **33** (5), 1084–1099.
- (a) C. B. Aakeröy *J. Chem. Soc., Chem. Commun.* **1998**, 1067–1068; (b) V. A. Russell, C. C. Evans, W. Li, and M. D. Ward, *Science*, **1997**, 276, 575–579; (c) L. Pan, X. Y. Huang, and J. Li, *J. Solid. State Chem.*, 2000, **152**, 236–246; (d) L. Pan, T. Frydel, M. B. Sander, X. Y. Huang, J. Li, *Inorg. Chem.* **2001**, 40, 1271–1283; (e) Y. B. Go, X. Q. Wang, E. V. Anokhina, and A. J. Jacobson, *Inorg. Chem.* 2005, **44**, 8265–8271; (f) Y. V. Kokunov and Y. E. Gorbunova, *Russ. J. Inorg. Chem.* 2007, **52**, 1530–1535; (g) M. Sarkar, V. Bertolasi, D. Ray, *Eur. J. Inorg. Chem.* **2010**, 2530–2536.
- (a) S. K. Ghosh, G. Savitha, P. K. Bharadwaj, *Inorg. Chem.* 2004, **43**, 5495–5497. (b) J. W. Cheng, S. T. Zheng, G. Y. Yang, *Dalton Trans.* 2007, 4059–4066. (c) Y. Q. Huang, Z. L. Shen, T. Okamura, Y. Wang, X. F. Wang, W. Y. Sun, J. Q. Yu, N. Ueyama, *Dalton Trans.* 2008, 204–213. (d) M. Du, X. J. Jiang, X. J. Zhao, *Inorg. Chem.* 2006, **45**, 3998–4006. (e) P. M. Forster, N. Stock, A. K. Cheetham, *Angew. Chem. Int. Ed.* 2005, **44**, 7608–7611. (f) P. M. Foster, A. R. Burbank, C. Livage, G. Ferey, A. K. Cheetham, *Chem. Commun.* 2004, 368–369. (g) M. L. Tong, S. Kitagawa, H. C. Chang, M. Ohba, *Chem. Commun.* 2004, 418–419. (h) P. Mahata, A. Sundaresan, S. Natarajan, *Chem. Commun.* 2007, 4471–4473. (i) W. X. Chen, S. T. Wu, L. S. Long, R. B. Huang, L. S. Zheng, *Cryst. Growth Des.* 2007, **7**, 1171–1175.
- (a) J. K. Tang, I. Hewitt, N. T. Madhu, G. Chastanet, W. Wernsdorfer, C. E. Anson, C. Benelli, R. Sessoli, A. K. Powell, *Angew. Chem., Int. Ed.*, 2006, **45**, 1729–1733. (b) B. Hussain, D. Savard, T. J. Burchell, W. Wernsdorfer, M. Murugesu, *Chem. Commun.* 2009, **9**, 1100–1102.
- X. P. Yang, R. A. Jones, M. J. Wiester, *Dalton Trans.* 2004, 1787–1788.
- J. P. Costes, L. Vendier, *Eur. J. Inorg. Chem.* 2010, 2768–2773.

11. (a) J. P. Costes, F. Dahan, F. Nicodeme, *Inorg. Chem.* 2001, **40**, 5285–5287; (b) A. K. Chaudhari, B. Joarder, E. Rivire, G. Rogez, S. K. Ghosh, *Inorg. Chem.* 2012, **51**, 9159–9161.
12. M. Lalia-Kantouri, C. D. Papadopoulos, A. G. Hatzidimitriou, S. Skoulika, *Struct. Chem.* 2009, **20**, 177–184.
13. (a) S. Ghelengi, H. Kargar, Z. Sharafi, R. Kia, *Acta Cryst.* 2011, **E67**, m1393; (b) Z. Q. Han, *Acta Cryst.* 2008, **E64**, m592; (c) R. Kia, H. Kargar, K. Zare, I. U. Khan, *Acta Cryst.* 2010, **E66**, m366.
14. S.-H. Zhang, R.-X. Zhao, G. Li, H. Y. Zhang, Q.-P. Huang, F. P. Liang, *J. Solid State Chem.*, 2014, **220**, 206–212.
15. G.M. Sheldrick, *Acta Cryst.* 2008, **A64**, 112–122.
16. (a)H. H. Zou, C. Feng, S. H. Zhang, Y. G. Wang, Y. Xiao, *Struct Chem.* 2011, **22**, 135–140. (a)P. Even, B. Boitrel, *Coord. Chem. Rev.* 2006, **250**, 519–541; (c)S. Yamada, *Coord. Chem. Rev.* 1999, **190**, 537–555. (d)Y. D. Zhang, S. H. Zhang, C. M. Ge, Y. G. Wang, Y. H. Huang, H. P. Li, *Synth. React. Inorg. Met. Org. Chem.* 2013, **43**(8), 990–994.
17. (a)S. T. Meally, C. McDonald, G. Karotsis, G. S. Papaefstathiou, E. K. Brechin, P. W. Dunne, P. McArdle, N. P. Power, L. F. Jones, *Dalton Trans.* 2010, **39**, 4809–4816. (b) W. L. Leong, J. J. Vittal, *New J. Chem.* 2010, **34**, 2145–2152. (c) L. Yang, Q. P. Huang; C. L. Zhang, R. X. Zhao, Zhang, *Supramol. Chem.*, 2014, **26**(2), 81–87.
18. (a)M. A. Bolcar, S. M. J. Aubin, K. Foltling, D. N. Hendrickson, G. Christou, *Chem. Commun.* 1997, 1485–1486. (b) R.W. Saalfrank, T. Nakajima, N. Mooren, A. Scheurer, H. Maid, F. Hampel, C. Trieflinger, J. Daub, *Eur. J. Inorg. Chem.* 2005, 1149–1153. (c) G. L. Abbati, A. Cornia, A. C. Fabretti, A. Caneschi, D. Gatteschi, *Inorg. Chem.* 1998, **37**, 3759–3766. (d) S. Koizumi, M. Nihei, M. Nakano, H. Oshio, *Inorg. Chem.* 2005, **44**(5), 1208–1210. (e) S. H. Zhang, C. Feng, *J. Mol. Struct.* 2010, **977**, 62–66. (f) S. Y. Chen, C. C. Beedle, P. R. Gan, G. H. Lee, S. Hill, E. C. Yang, *Inorg. Chem.* 2012, **51**, 4448–4457. (g), S. K. Langley, N. F. Chilton, B. Moubaraki, K. S. Murray, *Dalton Trans.* 2012, **41**, 9789–9796. (g) T. Liu, B. W. Wang, Y. H. Chen, Z. M. Wang, S. M. Wang, S. Gao, *Z. Anorg. Allg. Chem.* 2008, **634**, 778–783. (h) S. Koizumi, M. Nihei, T. Shiga, M. Nakano, H. Nojiri, R. Bircher, O. Waldmann, S. T. Ochsenein, H. U. Gudel, F. Fernandez-Alonso, H. Oshio, *Chem. Eur. J.* 2007, **13**, 8445–8453. (i) R. W. Saalfrank, A. Scheurer, R. Prakash, F. W. Heinemann, T. Nakajima, F. Hampel, R. Leppin, B. Pilawa, H. Rupp, P. Muller, *Inorg. Chem.* 2007, **46**, 1586–1592.
19. M. Tesmer, B. Muller, H. Vahrenkamp, *Chem. Commun.* 1997, 721–722.
20. (a)H. Oshio, N. Hoshino, T. Ito, M. Nakano, F. Renz, P. Gutlich, *Angew. Chem. Int. Ed. Engl.* 2003, **42**, 223–225. (b) G. Labat, C. Boscovic, H. U. Gudel, *Acta Cryst.* 2005, **E61**, m611–m613. (c) N. Hoshino, A. M. Ako, A. K. Powell, H. Oshio, *Inorg. Chem.* 2009, **48**, 3396–3407.
21. (a) V. Tudor, G. Marin, F. Lloret, V. C. Kravtsov, Y. A. Simonov, M. Julve, M. Andruh, *Inorg. Chim. Acta*, 2008, **361**, 3446–3452. (b) L. F. Chibotaru, L. Ungur, C. Aronica, H. Elmol, G. Pilet, D. Luneau, *J. Am. Chem. Soc.* 2008, **130**, 12445–12455. (c) A. Ferguson, A. Parkin, J. Sanchez-Benitez, K. Kamenev, W. Wernsdorfer, M. Murrie, *Chem. Commun.* 2007, 3473–3475. (d) R. Pattacini, P. Teo.; J. Zhang, Y. h. Lan, A. K. Powell, J. Nehrkorn, O. Waldmann, T. S. A. Hor, P. Braunstein, *Dalton Trans.* 2011, **40**, 10526–10534. (e) M. Moragues-Canovas, C. E. Talbot-Eeckelaers, L. Catala, F. Lloret, W. Wernsdorfer, E. K. Brechin, T. Mallah, *Inorg. Chem.* 2006, **45**, 7038–7040. (f) A. A. Kitos, C. G. Efthymiou, C. Papatriantafyllopoulou, V. Nastopoulos, A. J. Tasiopoulos, M. J. Manos, W. Wernsdorfer, G. Christou, S. P. Perlepes, *Polyhedron* 2011, **30**, 2987–2996. (g) S. T. Meally, C. McDonald, P. Kealy, S. M. Taylor, E. K. Brechin, L. F. Jones, *Dalton Trans.* 2012, **41**, 5610–5616. (h) X. T. Wang, B. W. Wang, Z. M. Wang, W. Zhang, S. Gao, *Inorg. Chim. Acta* 2008, **361**, 3895–3902. (i) W. Wang, H. Hai, S. H. Zhang, L. Yang, C. L. Zhang, *J. Cluster Sci.*, 2014, **25**(2), 357–365. (j) Q. P. Huang, G. Li, H. Y. Zhang, S.-H. Zhang, H. P. Li, *Z. Anorg. Allg. Chem.*, 2014, **640**(7), 1403–1407.
22. (a) Q. Gao, X. Q. Wang, M. T. Conato, T. Makarenko, A. J. Jacobson, *Cryst. Growth Des.* 2011, **11**, 4632–4638. (b) Y. Xiao, S. H. Zhang, G. Z. Li, Y. G. Wang, C. Feng, *Inorg. Chim. Acta.* 2011, **366**, 39–43.
23. K. O. Kongshaug, H. Fjellvåg, *Solid State Sci.* 2003, **5**, 303–310.
24. Forster, P. M.; Cheetham, A.K. *Microporous Mesoporous Mater.* 2004, **73**, 57–64.
25. Complex **a** can be prepared in a similar way than **1** except that Hheb was replaced by Hhmb. Green crystals of **a** were collected by filtration, washed with methanol and dried. Phase pure crystals of **a** were obtained by manual separation (yield: 278 mg, ca. 54.71 % based on Hhmb ligand). Crystal data for a heterometallic tetranuclear cluster **a**:  $C_{40}H_{40}Ni_2N_{10}Na_2O_{12}$ ,  $M_r = 1016.22 \text{ g mol}^{-1}$ , monoclinic,  $P2_1/C$ ,  $a = 13.405(1)$ ,  $b = 12.065(1)$ ,  $c = 14.665(1) \text{ \AA}$ ,  $\beta = 106.73(1)^\circ$ ,  $V = 2271.4(3) \text{ \AA}^3$ ,  $\theta = 26.32^\circ$ ,  $\lambda = 0.71073 \text{ \AA}$ ,  $T = 293 \text{ K}$ ,  $\mu(\text{Mo K}\alpha) = 0.920 \text{ mm}^{-1}$ . 9947 reflections were collected of which 4001 were unique ( $R_{int} = 0.0285$ ). The structure was solved by direct methods and refined by full-matrix least squares of  $F^2$ ,  $R_1 = 0.0436 (I > 2\sigma(I))$ ,  $wR_2 = 0.1501$  (all data). Max/min residual electron density  $0.464$ – $0.358 \text{ e \AA}^{-3}$  and the structure of (a) see Figure S4.
26. Complex **b** can be prepared in a similar way than **a** except that  $Ni(\text{ClO}_4)_2 \cdot 6\text{H}_2\text{O}$  was replaced by  $\text{Co}(\text{ClO}_4)_2 \cdot 6\text{H}_2\text{O}$ . Red crystals of **b** were collected by filtration, washed with methanol and dried. Phase pure crystals of **2** were obtained by manual separation (yield: 243 mg, ca. 47.80 % based on Hhmb ligand). Crystal data for a heterometallic tetranuclear cluster **a**:  $C_{40}H_{40}Co_2N_{10}Na_2O_{12}$ ,  $M_r = 1016.66 \text{ g mol}^{-1}$ , monoclinic,  $P2_1/C$ ,  $a = 13.345(2)$ ,  $b = 12.088(2)$ ,  $c = 14.716(2) \text{ \AA}$ ,  $\beta = 106.13(1)^\circ$ ,  $V = 2280.6(5) \text{ \AA}^3$ ,  $\theta = 28.99^\circ$ ,  $\lambda = 0.71073 \text{ \AA}$ ,  $T = 293 \text{ K}$ ,  $\mu(\text{Mo K}\alpha) = 0.818 \text{ mm}^{-1}$ . 7824 reflections were collected of which 3907 were unique ( $R_{int} = 0.1519$ ). The structure was solved by direct methods and refined by full-matrix least squares of  $F^2$ ,  $R_1 = 0.0939 (I > 2\sigma(I))$ ,  $wR_2 = 0.2689$  (all data). Max/min residual electron density  $0.838$ – $0.517 \text{ e \AA}^{-3}$  and the structure of (a) see Figure S4.
27. A. Sieber, C. Boskovic, R. Bircher, O. Waldmann, S. T. Ochsenein, G. Chaboussant, H. U. Gudel, N. Kirchner, J. V. Slageren, W. Wernsdorfer, A. Neels, H. Stoeckli-Evans, S. Janssen, F. Juranyi, H. Mutka, *Inorg. Chem.* 2005, **44**, 4315–4325.
28. M. A. Halcrow, J. C. Huffman, G. Christou, *Angew. Chem. Int. Ed.* 1995, **34**, 889–91.
29. (a) M. A. Halcrow, J. S. Sun, J. C. Huffman, G. Christou, *Inorg. Chem.* 1995, **34**, 4167–4177. (b) B. Cage, F. A. Cotton, N. S. Dalal, E. A. Hillard, B. Rakvin, C. M. Ramsey, *J. Am. Chem. Soc.* 2003, **125**, 5270–5271. (c) L. Feng, C. C. Beedle, W. Wernsdorfer, C.

- Koo, M. Nakano, S. Hill, D. N. Hendrickson, *Inorg. Chem.* 2007, **46**, 8126–8128. (d) M. L. Tong, M. Monfort, J. M. C. Juan, X. M. Chen, X. H. Bu, M. Ohba, S. Kitagawa, *Chem. Commun.* 2005, **2**, 233–235.
30. Y. Song, P. Zhang, X. M. Ren, X. F. Shen, Y. Z. Li, X. Z. You, *J. Am. Chem. Soc.* 2005, **127**, 3708–3709.
31. (a) G. Aromí, H. Stoeckli-Evans, S. J. Teat, J. Cano, J. Ribas, *J. Mater. Chem.* 2006, **16**, 2635–2644. (b) B. N. Figgis, M. Gerloch, J. Lewis, F. E. Mabbs, G. A. Webb, *J. Chem. Soc. A* 1968, 2086–2093.
32. E. K. Brechin, O. Cador, A. Caneschi, C. Cadiou, S. G. Harris, S. Parsons, M. Vonci, R. E. P. Winpenny, *Chem. Commun.* 2002, 1860–1861.
33. Y. Z. Zhang, W. Wernsdorfer, F. Pan, Z. M. Wang, S. Gao, *Chem. Commun.* 2006, **31**, 3302–3304.
34. (a) M. Murrie, S. J. Teat, H. Stoeckli-Evans, H. U. Güdel, *Angew. Chem. Int. Ed.* 2003, **42**, 4653–4656. (b) E. C. Yang, D. N. Hendrickson, W. Wernsdorfer, M. Nakano, L. N. Zakharov, R. D. Sommer, A. L. Rheingold, M. Ledezma-Gairaud, G. J. Christou, *Appl. Phys.* 2002, **91**, 7382–7384.

## Figures captions

Scheme 1. Coordination mode of the ligand.

Scheme 2. pH and temperature effects on the structural variations from heterometallic heptanuclear or heptanuclear clusters to cubane clusters based on 2-hydroxy-3-ethoxy-benzaldehyde.

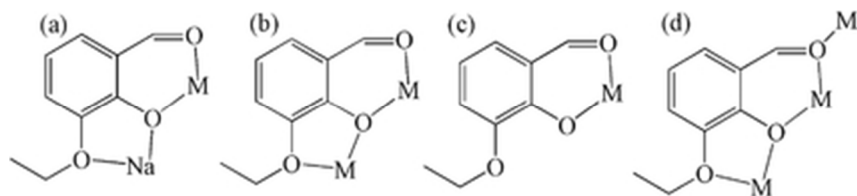
Figure 1. The anion structures of  $[M_4Na_3(\text{heb})_6(\text{N}_3)_6]^-$  ( $M = \text{Ni}$  (**1**),  $\text{Co}$  (**2**)). All H-atoms were omitted for better clarity.

Figure 2. Molecular structure of **3**. All H-atoms were omitted for better clarity.

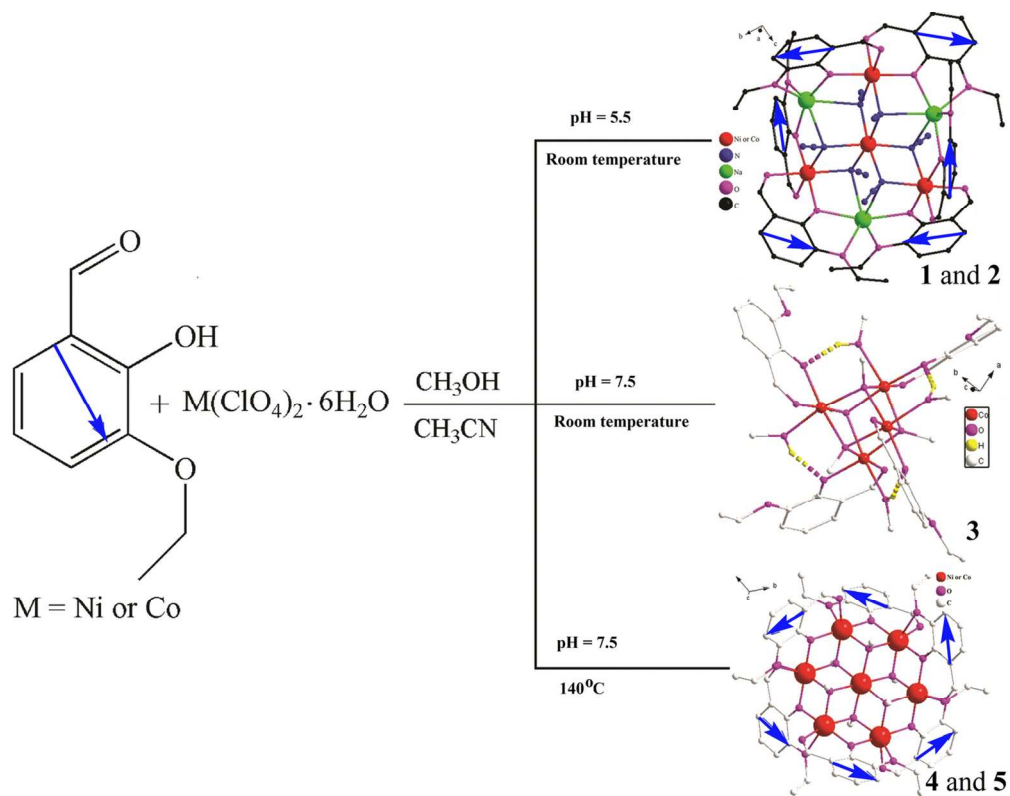
Figure 3. The cation structures of  $[M_7(\text{heb})_6(\mu_3\text{-OCH}_3)_6]^{2+}$  ( $M = \text{Ni}$  (**4**), and  $\text{Co}$  (**5**)). All H-atoms were omitted for better clarity.

Figure 4. Plots of  $\chi_M T$  and  $\chi_M$  vs  $T$  measured in a 1000 Oe field for **1**(a) and **4**(b).

Figure 5. Plots of  $\chi_M T$  and  $\chi_M$  vs  $T$  measured in a 1000 Oe field for **2**(a), **3** (b), and **5**(c). The solid lines represent the best fits of data between 300 and 50 K as described in the text for **3**.



Scheme 1. Coordination mode of the ligand.  
17x4mm (600 x 600 DPI)



Scheme 2. pH and temperature effects on the structural variations from heterometallic heptanuclear or heptanuclear clusters to cubane clusters based on 2-hydroxy-3-ethoxy-benzaldehyde.  
62x49mm (600 x 600 DPI)

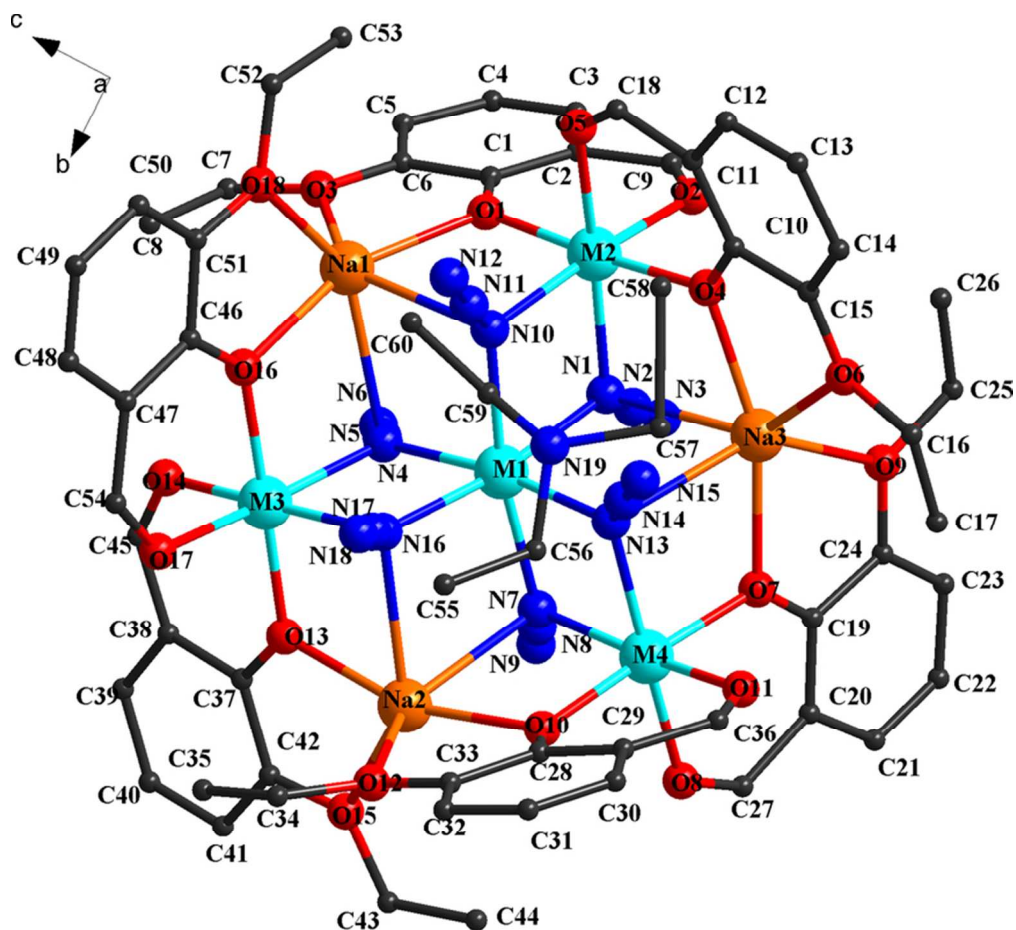


Figure 1. The anion structures of  $[M_4Na_3(heb)_6(N_3)_6]^-$  ( $M = Ni$  (1),  $Co$  (2)). All H-atoms were omitted for better clarity.  
73x67mm (300 x 300 DPI)

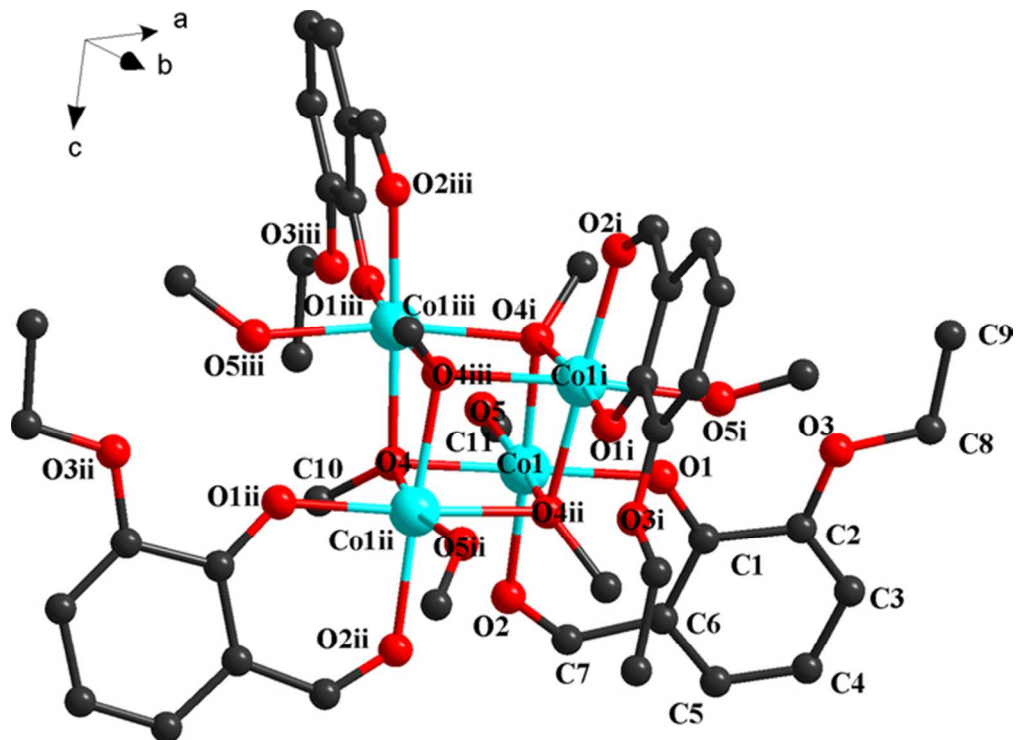


Figure 2. Molecular structure of 3. All H-atoms and water molecules were omitted for better clarity.  
59x43mm (300 x 300 DPI)

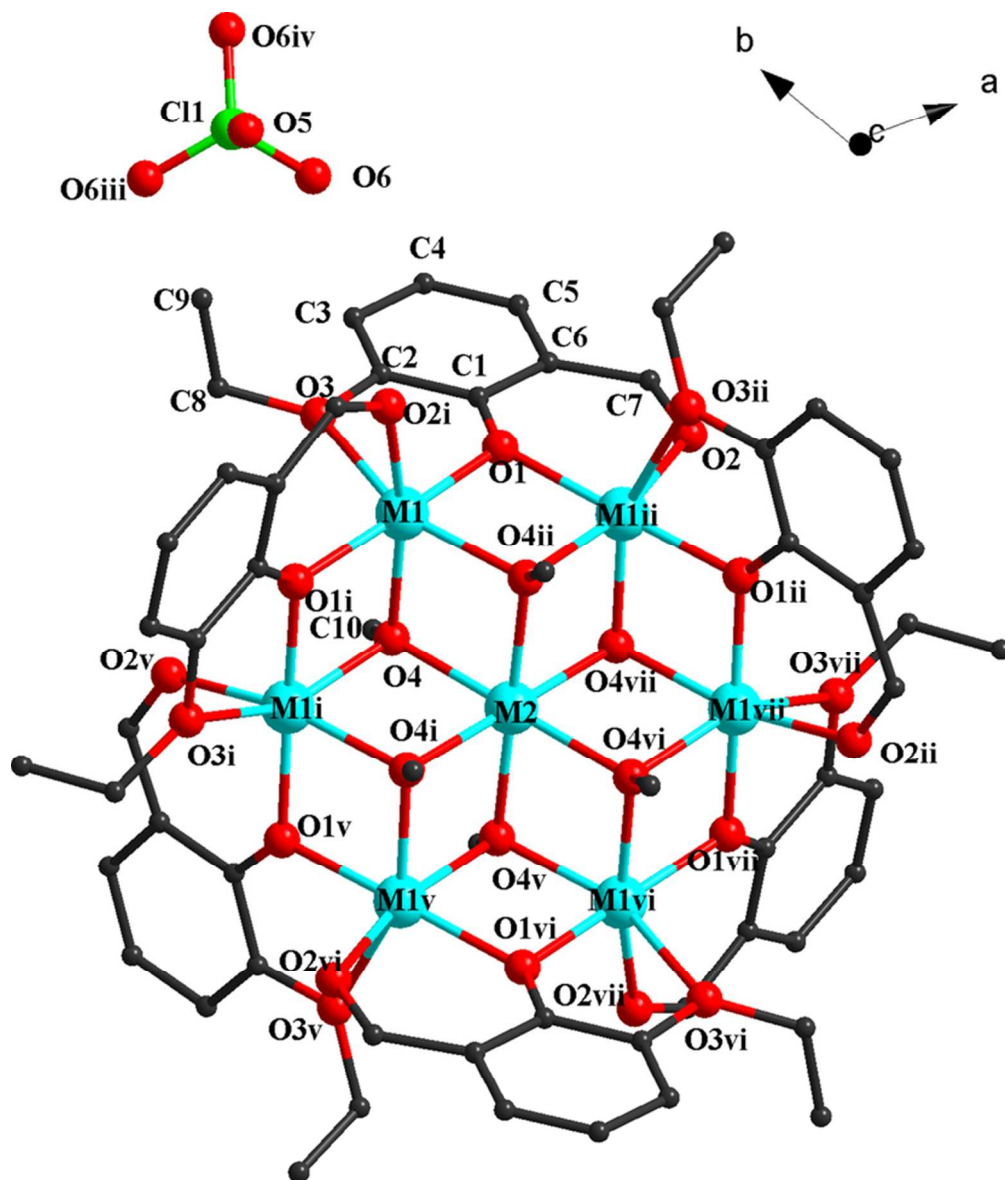


Figure 3. The cation structures of  $[M_7(\text{heb})_6(\mu^3\text{-OCH}_3)_6]^{2+}$  ( $M = \text{Ni}$  (4), and  $\text{Co}$  (5)). All H-atoms were omitted for better clarity.  
70x82mm (300 x 300 DPI)

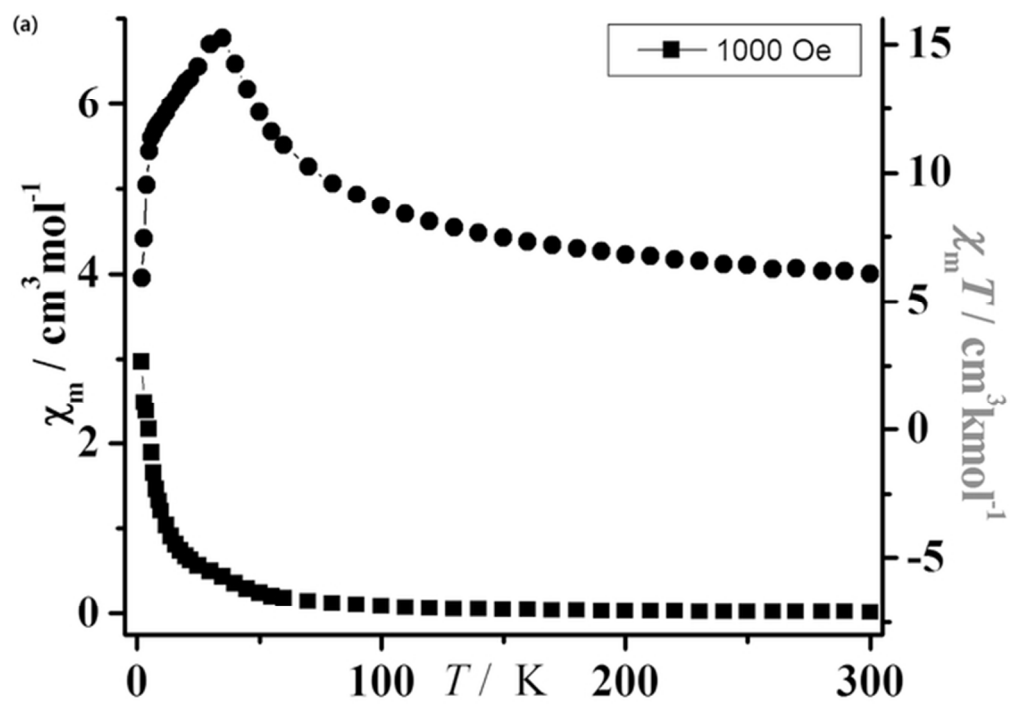


figure 4a  
56x40mm (300 x 300 DPI)

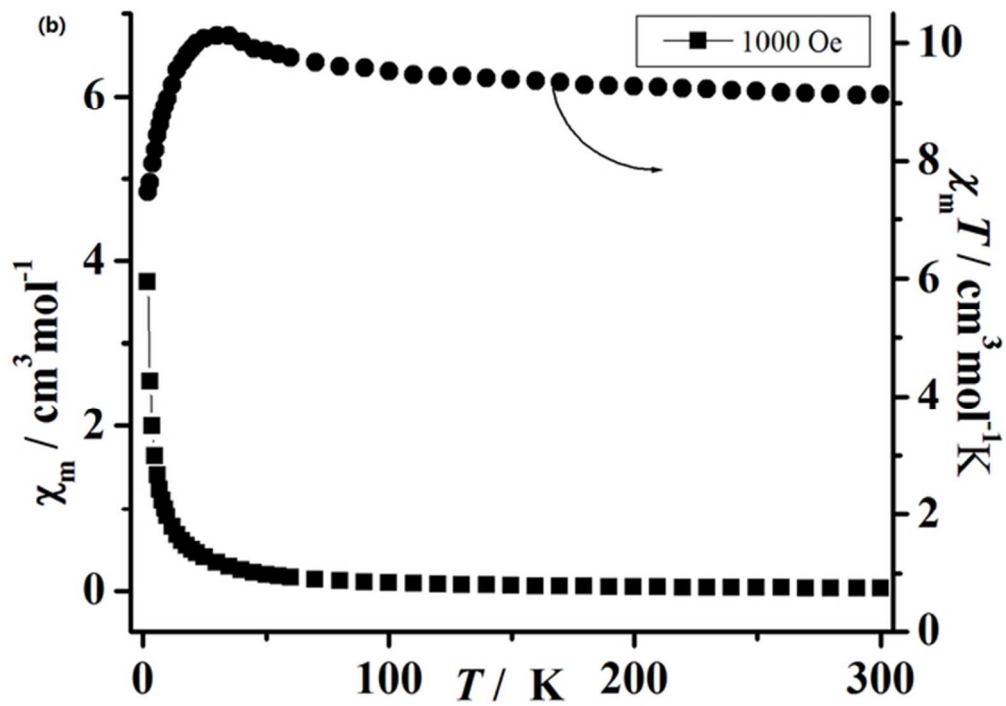


Figure 4. Plots of  $\chi_m T$  and  $\chi_m$  vs  $T$  measured in a 1000 Oe field for 1(a) and 4(b).  
56x39mm (300 x 300 DPI)

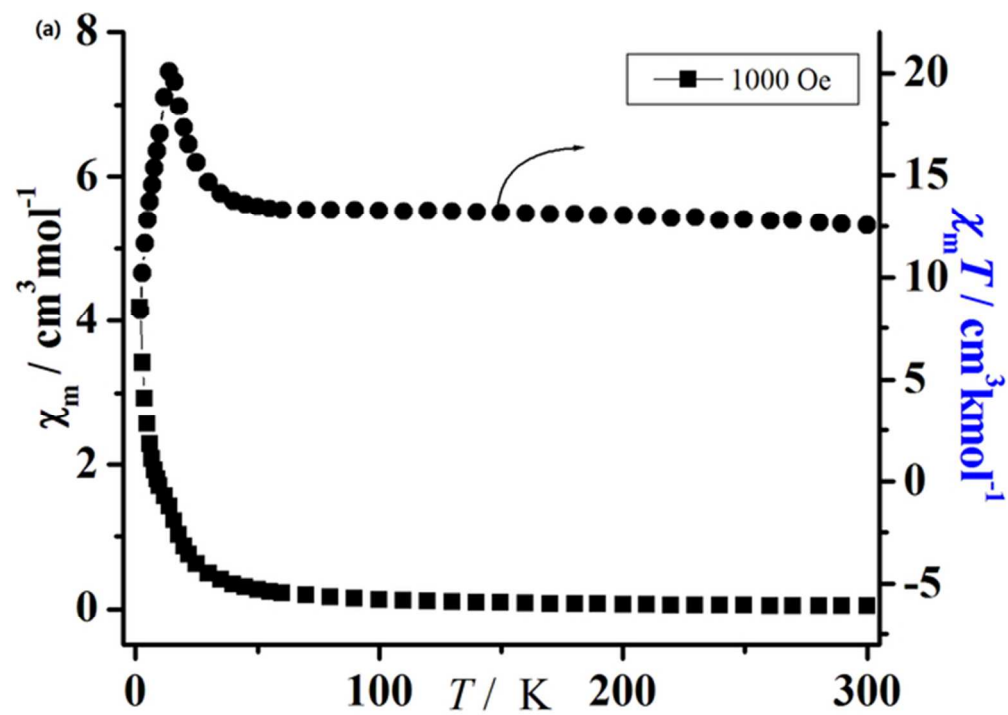


figure 5a  
56x39mm (300 x 300 DPI)

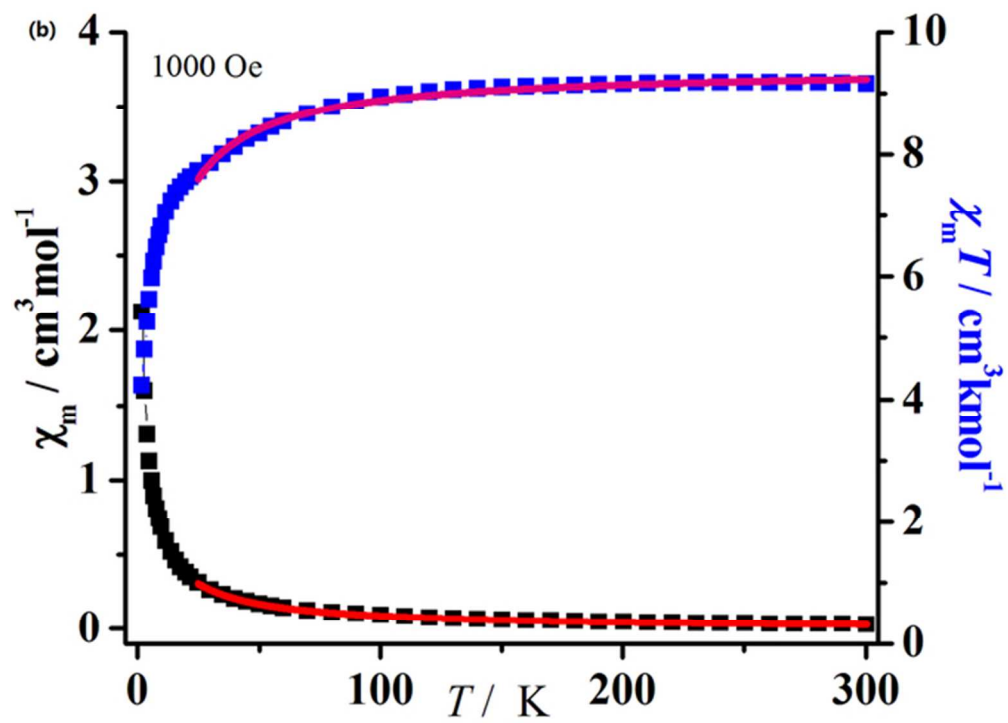


figure 5b  
57x40mm (300 x 300 DPI)

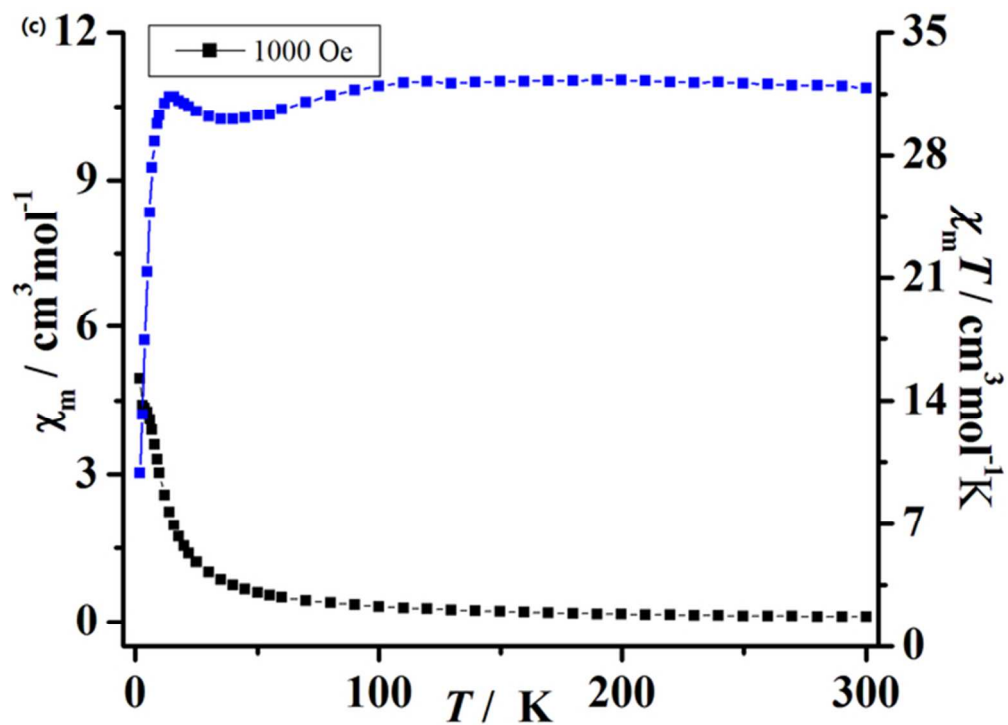


Figure 5. Plots of  $\chi_m T$  and  $\chi_m$  vs  $T$  measured in a 1000 Oe field for 2(a), 3 (b), and 5(c). The solid lines represent the best fits of data between 300 and 50 K as described in the text for 3.

57x41mm (300 x 300 DPI)